J. Min. Metall. Sect. B-Metall. 48 (3) B (2012) 461 - 469

Journal of Mining and Metallurgy, Section B: Metallurgy

MICROSTRUCTURE AND PROPERTIES DEGRADATION OF P/T 91, 92 STEELS WELDMENTS IN CREEP CONDITIONS

L. Falat[a], V. Homolová[a,*], J. Kepič[a], M. Svoboda[b], A. Výrostková[a]

[a] Institute of Materials Research, Slovak Academy of Sciences, Košice, Slovak Republic
[b] Institute of Physics of Materials, Academy of Sciences of the Czech Republic, Brno, Czech Republic

(Received 01 July 2012; accepted 10 September 2012)

Abstract

The studies were performed on dissimilar ferritic/austenitic weldments between 9Cr tempered martensitic steels of the grades either P/T 91 or 92 and unstabilised AISI316H austenitic steel. The welded joints were fabricated using the fusion welding by tungsten inert gas (TIG) method with Ni-based filler metal. Microstructural analyses were performed using light and electron microscopy. Microstructural gradient in heat-affected zone (HAZ) of 9Cr steels remained preserved during creep exposure. All weldments fractured by the type IV failure within their intercritical HAZ (ICHAZ) regions. The most remarkable microstructural change during creep was the precipitation of intermetallic Laves phase. Experimentally determined phases of the samples after creep exposure are in good agreement with equilibrium thermodynamic calculations.

Keywords*: Dissimilar weldments; Microstructure; Creep behaviour; Phase composition; Thermodynamic calculations*

1. Introduction

Demands on the increase of thermal efficiency in power plants have been the main driving force for research and development of high temperature creep-resistant steels during several last decades [1]. Newly developed creep-resistant steels are already used at ultra supercritical (USC) conditions (600 °C, 25 – 30 MPa) in the most modern power stations throughout the world. Currently, much effort is being put into development of creep and corrosion-resistant steels for application at a new class USC conditions (650 °C, 30 - 35 MPa) [2]. This development involves both ferritic and austenitic steels. The most critical construction parts in steam boilers are bends and welded joints [3]. Since these boilers consist of the circuits heated up to different temperatures, dissimilar materials such as ferritic and austenitic steels are used for their construction. Although the ferritic steels are in principle inferior in creep strength to the austenitic steels, they are superior in thermal properties such as thermal expansivity and conductivity [4]. Whereas in a primary part of supercritical steam boiler Cr-Mo ferritic steels are used for water evaporators and steam headers [5], in high temperature part of superheaters and reheaters Cr-Ni austenitic steels are employed [6]. Thus, the joining of dissimilar steels is unavoidable in boiler system of power plants. Classical fusion welding using tungsten inert gas (TIG) method still belong to the most frequently used procedures for commercial production of weldments for power-related as well as petrochemical industry [7].

The first dissimilar ferritic/austenitic weldments were manufactured with austenitic steel filler materials [8]. The primary use of austenitic welding consumables enabled the joining of ferrite and austenite, but afterwards several problems have been encountered in these welds. In metallurgical point of view, the austenitic fillers were problematic due to their high susceptibility to solidification cracking [8]. In addition, their creep lives were found to be remarkably shorter than expected, only about one third of their design life. It was found that there were two main reasons for this behaviour. The first one was the existence of thermally induced cyclic stresses due to remarkable difference in thermal expansivity between ferrite and austenite. The second one was related to the formation of soft carbon-depleted zone at the ferritic side of the ferritic/austenitic interface due to carbon migration from ferritic steel to austenitic weld metal, driven by carbon activity gradient [9]. To overcome the problems with austenitic steel filler materials, alternative Ni-based welding consumables of Inconel-type have been introduced [10]. The main benefits of Ni-based weld metals (Ni WM) come from their thermal properties which lie in between of the thermal properties related to ferrite and austenite, respectively. Thus the

* *Corresponding author: vhomolova@imr.saske.sk*

DOI:10.2298/JMMB120701057F

Dedicated to the memory of Professor Zbigniew Moser

amplitude of cyclic thermal stresses is rapidly reduced due to the more gradual variation in thermal properties throughout the dissimilar weldment [8]. Another beneficial feature of Ni-based fillers is their low carbon solubility, so they act like carbon diffusion barrier [10] and hence carbon depletion at the ferritic steel side of dissimilar welded joint is considerably suppressed. In this manner, the creep resistance of the ferritic/austenitic weldments with Ni WM was significantly improved, compared to the welds produced with austenitic steel welding consumables.

The present study was carried out to characterise the microstructure and creep behaviour of experimental ferritic/austenitic welded joints between the 9Cr steels (either *T91* or *T92*) and the unstabilised austenitic steel (*AISI316H*), welded with Ni-based welding consumables.

2. Experimental

The experimental weldments were fabricated by the company *SES a. s. Tlmače, Slovak republic*. The original tubes of base materials, i.e. *T91*, *T92*, and *AISI316H* were supplied from the producers Vallourec & Mannesman, Tenaris Dalmine, and Sandvik, respectively. The dimensions of the tubes were: 38 mm outer diameter and 5.6 mm wall thickness. The dissimilar welded joints *T91+AISI316H* and *T92+AISI316H* were welded using the Ni-based filler materials *Thermanit Nicro 82* and *Nirod 600*, respectively. The chemical compositions of base materials (BM) and filler materials used for production of the studied weldments are given in Tables 1 and 2. Preparation of welding edges and sequence of welding passes were in principle the same for all investigated weldments (see Fig. 1). Welding parameters for the production of ferritic/austenitic weldments were: welding current 70-110 A, voltage 12-17 V and heat input 9-12 kJ/cm. The diameter of TIG electrode was 2.4 mm. Post-weld heat treatments (PWHT) of all weldments were performed in conventional way, i.e. by subcritical tempering at 750-760 °C for 1 h with controlled heating and cooling rates of 150 °C/h.

All experimental studies were performed using cross-weld (c-w) samples. The prepared tubular weldments were cut by spark erosion into the c-w blocks, as schematically shown in Fig. 2. The blocks were then used for the machining of cylindrical tensile creep samples with a body diameter of 4 mm, gauge length of 40 mm and M6 head thread. The creep strain was measured at frequency of 1/h using linear variable displacement transducers (LVDT) linked with computer data collection system. The gauge

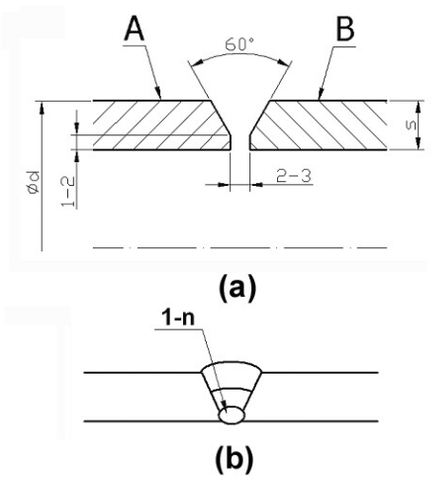

Figure 1. *Schematic preparation of welding edges (a) and welding design (b).*

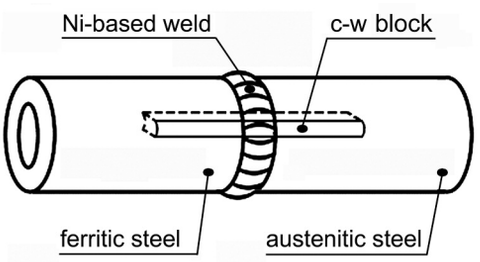

Figure 2. *Schematic cross-weld (c-w) sampling.*

Table 1. *Chemical compositions of the base materials / wt.%*

	C	N	Si	Mn	P	S	Cr	Mo	W	B	Ni	Al	V	Nb	Fe
T91	0.092	0.045	0.39	0.44	0.011	0.003	8.68	0.92	-	-	0.25	0.015	0.2	0.064	Bal.
T92	0.11	0.056	0.38	0.49	0.019	0.002	9.08	0.31	1.57	0.0023	0.33	0.014	0.2	0.069	Bal.
AISI 316H	0.052	-	0.51	1.77	0.031	0.006	16.76	2.05	-	-	11.13	-	-	-	Bal.

Table 2. *Chemical compositions of the Ni-based filler materials / wt.%*

	C	Si	Mn	P	S	Cr	Mo	Ni	Nb	Ti	Cu	Fe
Th.Nicro82	0.011	0.07	3.21	0.004	0.001	20.71	0.004	Bal.	2.6	0.368	0.01	0.31
Nirod 600	0.05	0.3	3	0.03	0.015	20	-	Bal.	2	-	-	2

length of creep specimens included all dissimilar materials of the studied weldments. The minimum creep rates were determined from the linear portions of creep curves as their slopes. Microstructural analyses were carried out using light microscopy (LM), scanning electron microscopy (SEM) linked with energy dispersive X-ray spectroscopy (EDX). Thermodynamic calculations of phase equilibria were performed by the software Thermo-Calc [11] using thermodynamic database STEEL16 formulated by Kroupa [12,13].

3. Results and discussion

3.1 Microstructure in initial PWHT state

Figs. 3-7 represent the light-optical micrographs of different regions of weldments *T91+AISI316H* and *T92+AISI316H* in PWHT state. Tempered martensitic microstructures of unaffected *T91* and *T92* base materials are shown in Fig. 3a and b, respectively. The overall view on microstructures of *T91* and *T92* regions located close to their Ni WM regions are shown in Fig. 4a and b, respectively. Both of these regions consist of their coarse-grained (CGHAZ) and fine-grained (FGHAZ) sub-regions as a result of phase transformation behaviour of *T91*, *T92* steels. The detailed microstructures of *T91* and *T92* sub-regions are documented in Fig. 5a–d. It can be stated that general features of tempered martensitic microstructures related to mutually corresponding regions of *T91* and *T92* parts (i.e. T91 BM to T92 BM and T91 HAZs to T92 HAZs) of the studied weldments are very similar and basically they cannot be distinguished from each other by means of metallographic analysis.

The austenitic part of both weldments *T91+AISI316H* and *T92+AISI316H* showed identical microstructural features. The *AISI316H* base material is formed of recrystallized, roughly equiaxed, polygonal grains (Fig. 6a). Major intergranular and intragranular precipitates are $M_{23}C_6$ (M = Cr, Fe)

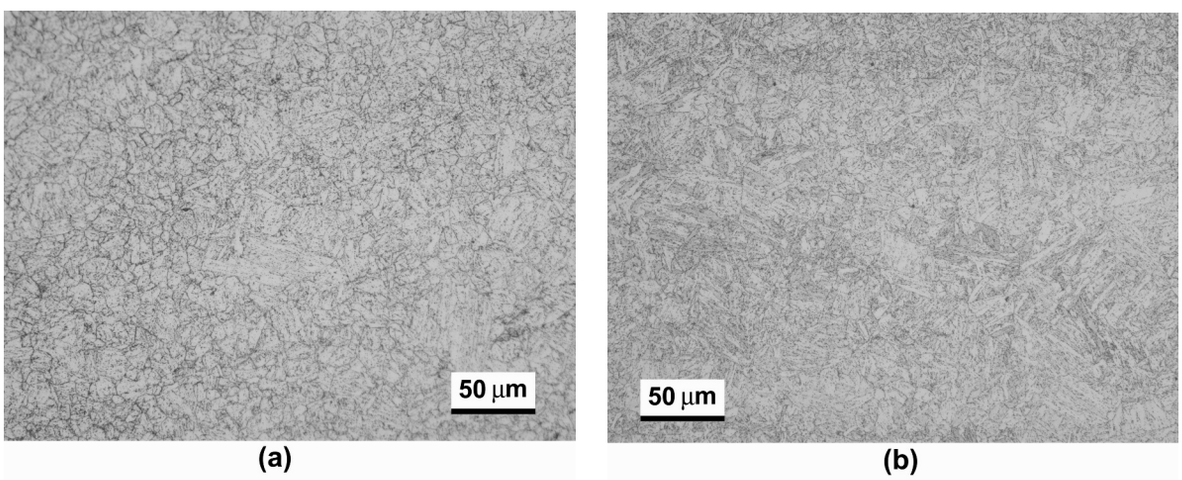

Figure 3. *Light-optical microstructures of the martensitic steels base materials: T91 BM (a), T92 BM (b).*

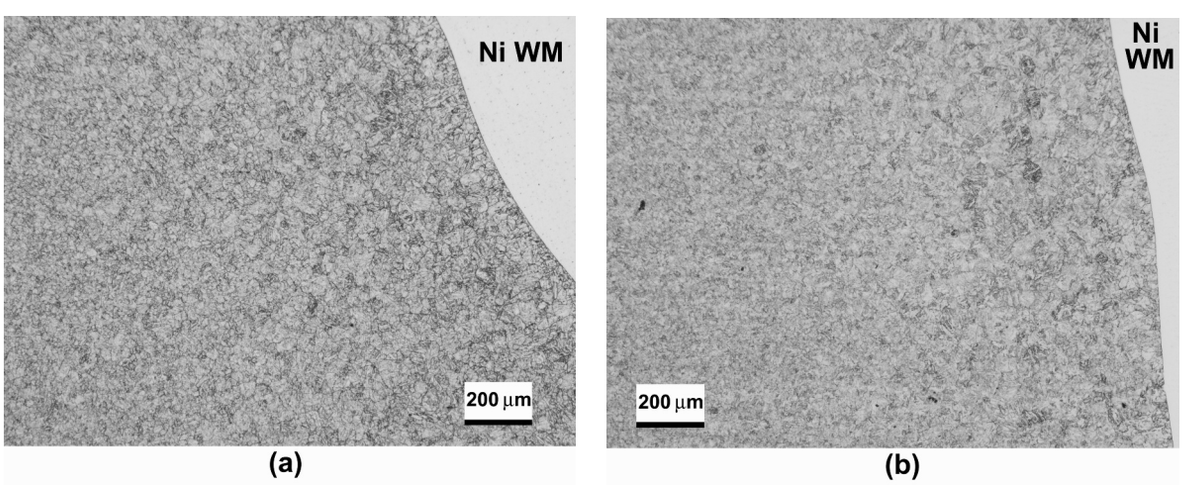

Figure 4. *Overall microstructures of the martensitic steels heat-affected zones: T91 HAZ (a), T92 HAZ (b).*

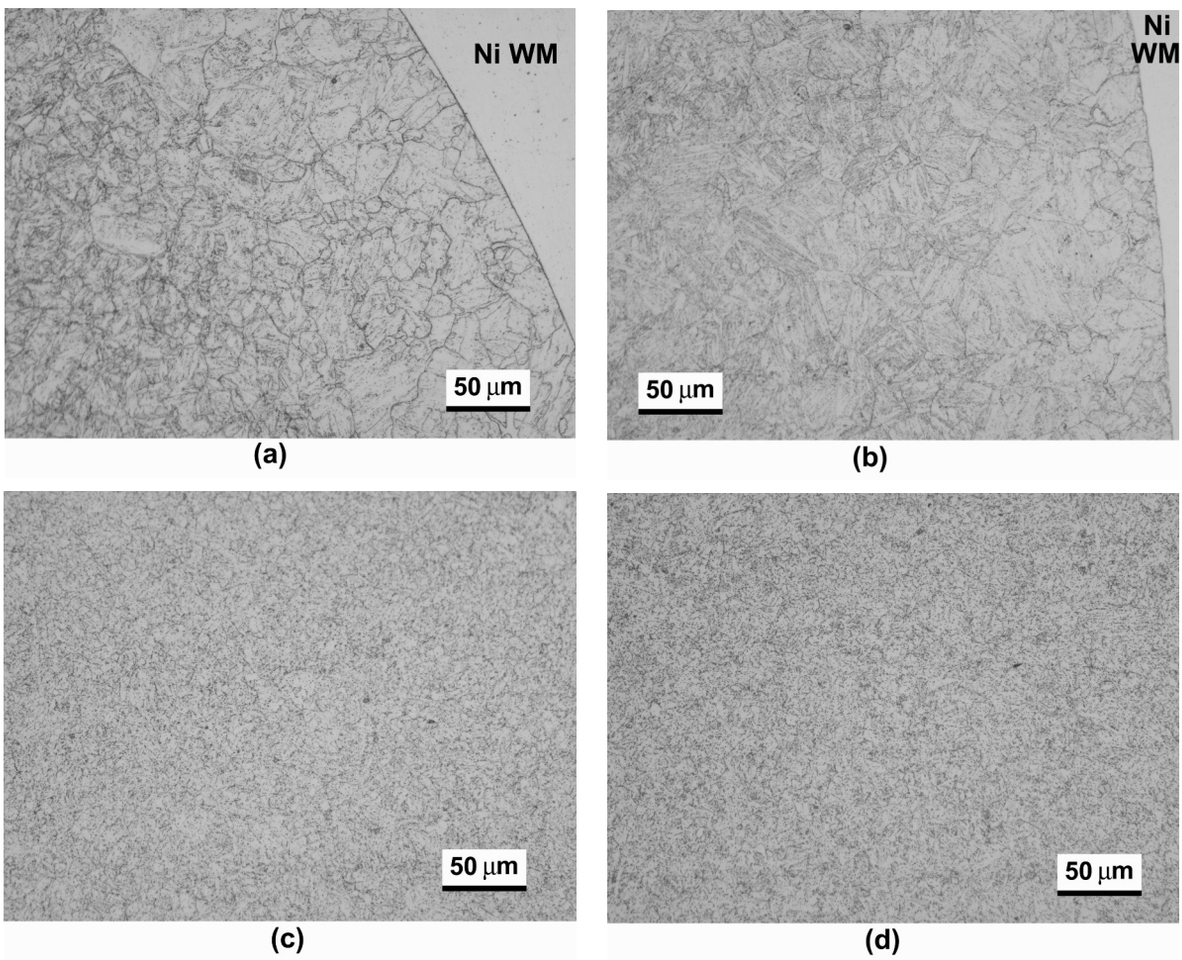

Figure 5. *Light-optical microstructures of the individual HAZ subregions of the martensitic steels: T91 CGHAZ (a), T92 CGHAZ (b) T91 FG/ICHAZ (c), T92 FG/ICHAZ (d).*

carbides [14]. The microstructure of *AISI316H* HAZ close to Ni WM is shown in Fig. 6b. Due to heat input during welding, polygonal grains of *AISI316H* HAZ are coarsened, compared to the unaffected microstructure of *AISI316H* BM (Fig. 6a). The austenitic steel HAZ is restricted to only a narrow region close to Ni WM due

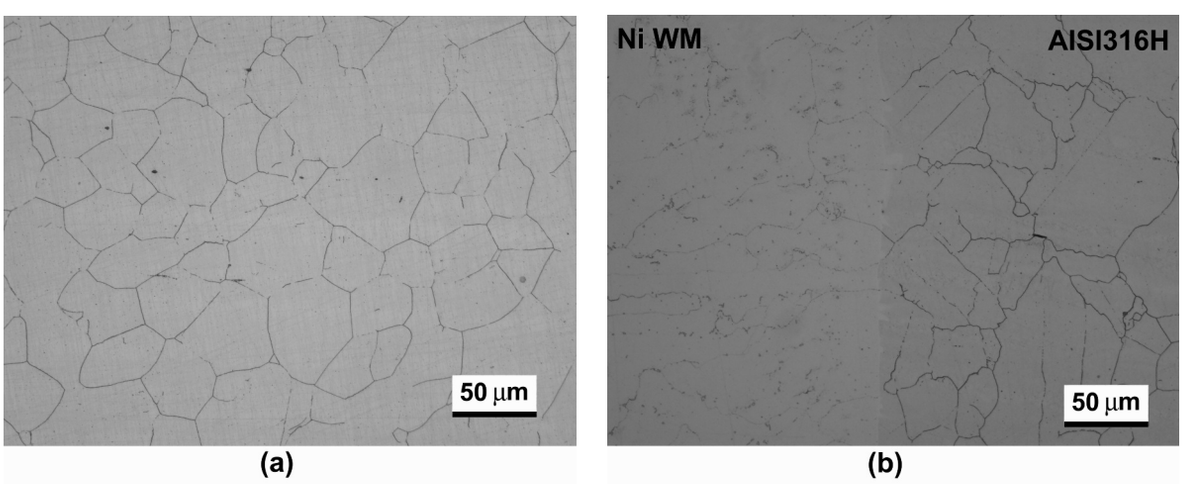

Figure 6. *Light-optical microstructures of the austenitic parts of the studied weldments: AISI316H BM (a), AISI316H HAZ (b).*

to relatively smaller thermal conductivity than that of the ferritic steel [4]. From Fig. 6b it is evident that the firstly solidified grains of Ni WM nucleated and grew epitaxially from the austenitic steel substrate. Thus the fully preserved continuation between the *AISI316H* steel grain boundaries and Ni WM solidification boundaries can be seen in Fig. 6b.

The microstructures of Ni WMs *Thermanit Nicro 82* and *Nirod 600* close to their interfaces with *T91* and *T92* steels are shown in Fig. 7a and b, respectively. Due to the heat transfer during cooling after the weldments fabrication, the Ni WMs grains are elongated towards martensitic steels base materials. The microstructures of Ni WMs contain intragranular as well as intergranular precipitates. In order to characterise the precipitates in Ni WMs, additional microstructural analyses were performed using SEM observations with EDX spectroscopy. For example, the characterisation of different morphologies of the precipitates in Nirod 600 weld metal is shown in Figs. 8 and 9. Both these precipitate types were found to be rich in Nb. With respect to the overall chemical composition of *Nirod 600* WM, these precipitates are indicated to be the NbC carbides. The same precipitates were indicated in *Thermanit Nicro 82* weld metal. Moreover, these precipitates were extracted in carbon replicas and analysed in TEM by SAED technique [15]. It has been confirmed that these precipitates exhibit face-centered cubic crystal structure.

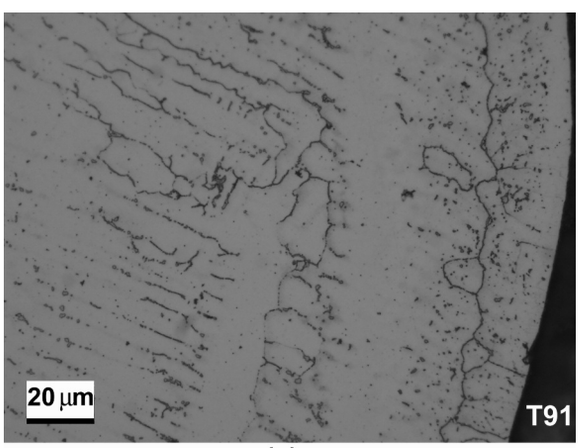

Figure 7. *Light-optical microstructures of Ni WMs of the studied weldments: Thermanit Nicro 82 (a), Nirod 600 (b).*

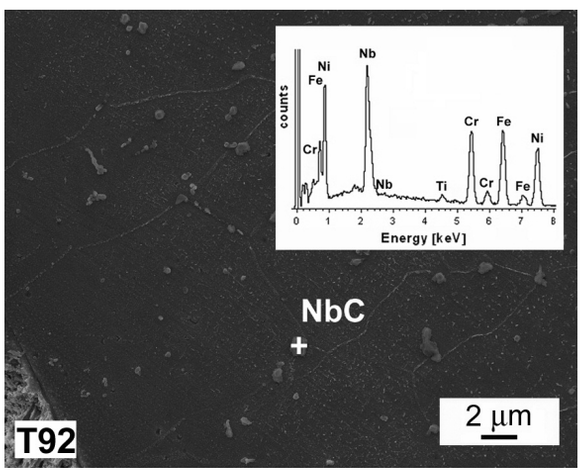

Figure 8. *Discrete round precipitate in Nirod 600 weld metal and its corresponding EDX spectrum.*

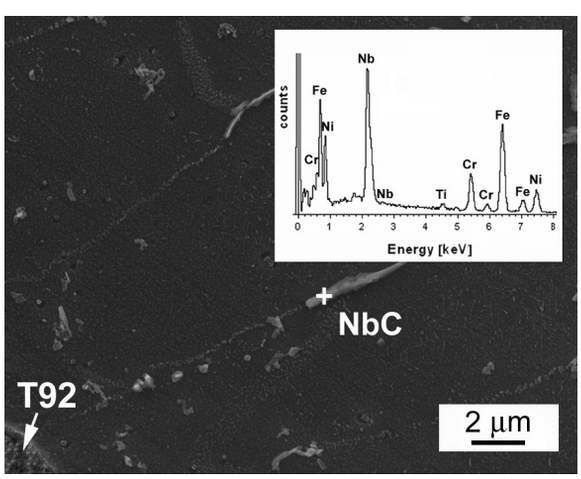

Figure 9. *Longitudinal, grain boundary precipitate in Nirod 600 weld metal and its corresponding EDX spectrum.*

3.2 Creep deformation behaviour

In this work the minimum creep rate was used as criterion of creep strength. Fig. 10 shows logarithmic dependencies of the secondary creep rate (ε_{min}) on applied stress (σ) at two creep temperatures for both studied

weldments. The stress exponents (n-values) are represented by the slopes of linear regressions to the dependences of $\log(\varepsilon_{min})$ vs. $\log(\sigma)$. For the weldment *T91+AISI316H* the values of stress exponents are 7.4 and 7.8 at temperatures 650 and 625 °C, respectively (see Fig. 10a). The obtained stress exponents of the investigated *T91+AISI316H* welded joint are in fairly good agreement with the n-value of 7.7 reported for the creep behaviour of P91 steel with simulated intercritical microstructure [16]. Fig. 10b shows the stress dependencies of minimum creep rates at different temperatures for the weldment *T92+AISI316H*. Since it was obvious that the data-points of the dependences in Fig. 10b did not lie on a single line, so-called „multi-region analysis" was used for the determination of stress exponents. Thus the regions with higher stress exponents (*n* about 12 ~ 13) correspond to the high stress regime (HSR), whereas the regions with lower stress exponents (*n* about 4 ~ 6) correspond to the low stress regime (LSR) of creep (Fig. 10b). It can be seen that the transition from HSR to LSR corresponds to the different stresses at different creep temperatures, namely 100 MPa at 650 °C and 120 MPa at 625 °C (see Fig. 10b). Kloc and Sklenička [17] reported the change from HSR to LSR to be at about 100 MPa for 9% Cr steels. Ennis et al. [18] reported the HSR-to-LSR transition for P92 steel to be at 120 and 160 MPa for the temperatures 650 and 600 °C, respectively, which qualitatively supports the tendency in creep behaviour observed also in this study, i.e. the increase in transition stress with decreasing temperature. The stress exponents reported by Ennis et al. [18] for tempered P92 steel are 6 and 16 for and , respectively. Lee et al. [19] published the *n*-values 8 and 17 for the low-stress long-term creep tests and for the high-stress short-term tests, respectively. The higher *n*-values reported by these authors [18,19] can be related to the higher applied stresses used in their studies. On the other hand, Sawada et al. [20] reported for P92 steel the stress exponent to be 12.7 in at 650 °C which is very similar value as obtained in this study (Fig. 10b). In most of literature studies, the creep mechanisms are not specifically discussed, or if so only the statements are given referring to the power-law creep controlled by dislocation-climb or thermally activated dislocation glide.

3.3 Creep fracture behaviour

Fig. 11 shows a profile view on the sub-fracture microstructures of two fracture counter-parts of the creep sample. It is obvious that the microstructural gradient consisting of CGHAZ, FGHAZ, ICHAZ and subcritical (SCHAZ) remained preserved even after creep exposure. The creep fracture location within the ICHAZ region corresponds to the „type IV cracking" failure mode. More detailed microstructural characterisation of the weld-joint *T91+AISI316H* after the creep test at 625 °C / 80 MPa was performed by SEM. Fig. 12a shows an intensive creep cavitation in the ICHAZ microstructure beneath the creep fracture. Fig. 12b indicates two types of precipitates in CGHAZ microstructure, namely the carbides ($M_{23}C_6$ and MX) and Laves phase (Fe_2Mo). From the fracture path it is obvious that the type IV failure is characterised by intergranular fracture caused by initiation and growth of creep voids and cracks. The precipitation of Fe_2Mo based Laves phase in T91 steel was also predicted by thermodynamic calculation (Fig. 13). Besides the intermetallic Laves phase, the $M_{23}C_6$ carbide and the MX carbonitride are also predicted at the given creep temperature (625 °C). The presence of Laves phase precipitates was confirmed by EDX analysis.

The failure by „type IV cracking" of the *T92+AISI316H* weld-joint after the creep test at 625 °C / 100 MPa with the life of 4060 h is shown in Fig. 14. The size and morphology of precipitates in the ICHAZ microstructure is visualised in more detail in Fig. 15. The smallest intragranular precipitates are generally known in T/P92 steels to be the MX carbonitrides. Besides these fine precipitates, two types of larger precipitates were distinguished using the contrast of back-scattered

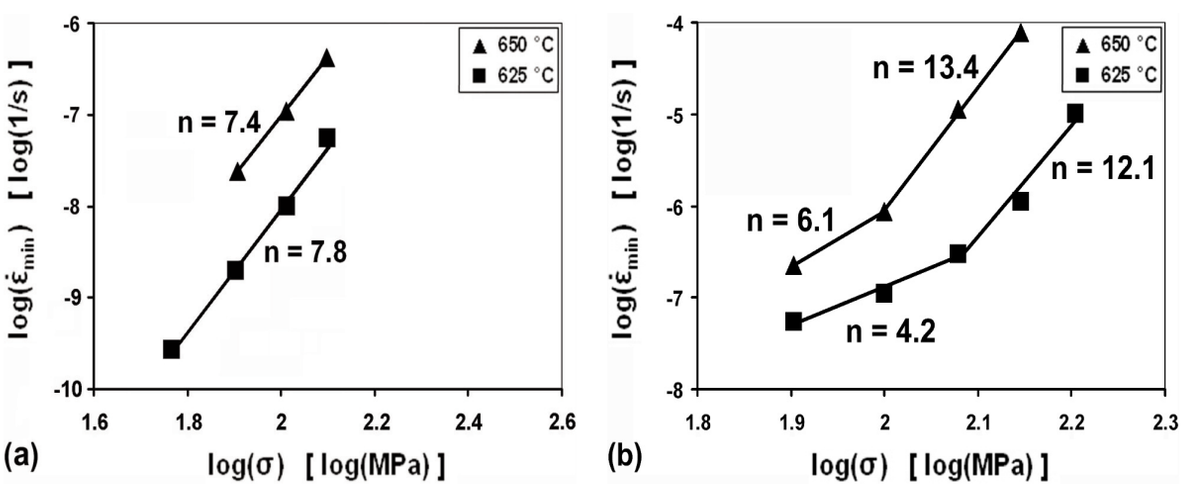

Figure 10. *Determination of stress exponents for the weldment T91+AISI316H (a) and the weldment T92+AISI316H (b).*

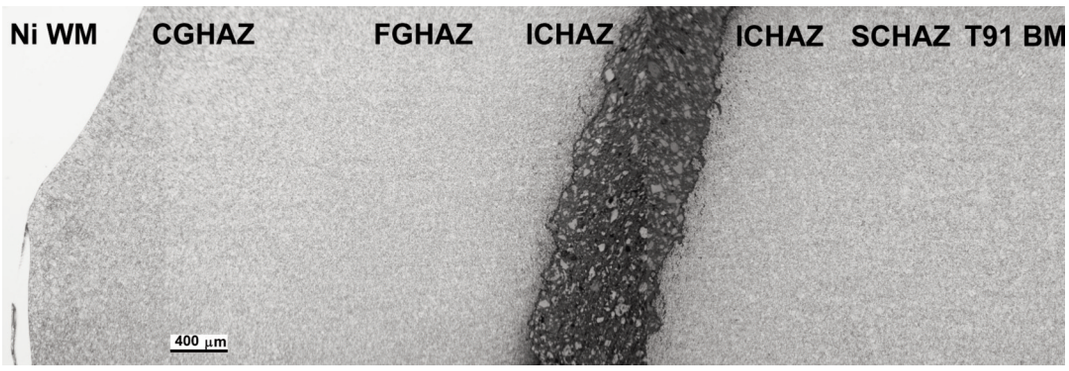

Figure 11. *Profile view on the sub-fracture microstructures of two counter-parts of the T91+AISI316H weld-joint ruptured by the „type IV cracking" failure after 1220 h of creep test at 625 °C / 80 MPa.*

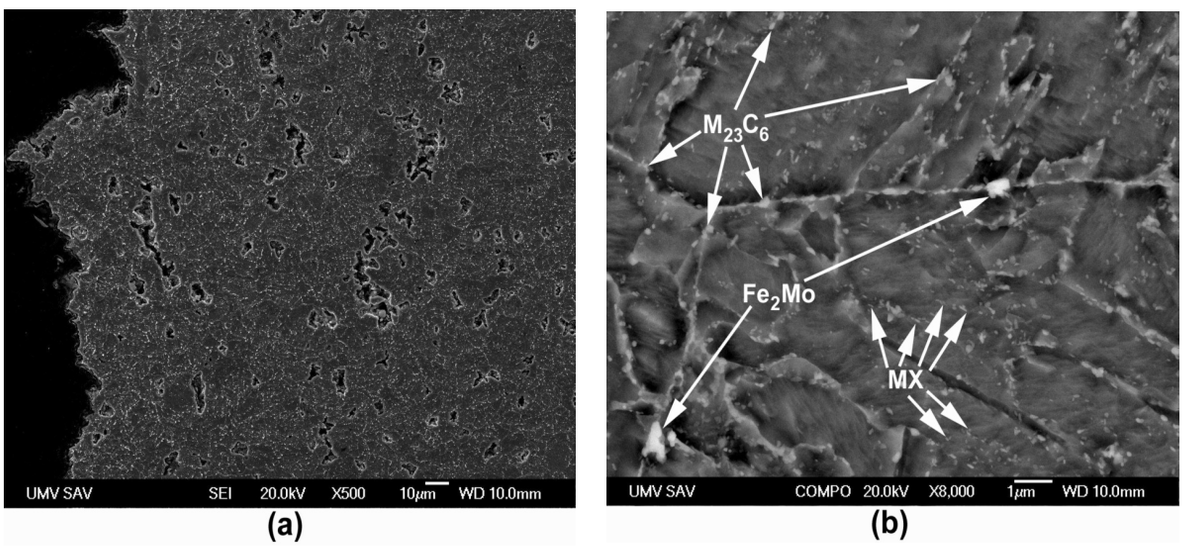

Figure 12. *Intensive cavitation in T91 fine-grained ICHAZ microstructure (a) and indication of the precipitates in CGHAZ microstructure using the contrast of back-scattered electrons in SEM (b).*

electrons (Fig. 15b). Since it is well-known that heavy elements like Mo, W give a bright contrast and the lighter elements like Cr give a less pronounced greyish contrast, a qualitative differentiation between the $Fe_2(W,Mo)$-based Laves phase and the Cr-rich $M_{23}C_6$ carbide was possible (see Fig. 15b). It is well-known that the coarsening of Laves phase $Fe_2(W,Mo)$ removes the atoms of Mo and W from solid solution and thus deteriorates the T92 steel creep strength. The presence of these secondary phases in microstructure of T92 steel was also confirmed by thermodynamic calculation using Thermo-Calc (Fig. 16). Fig. 16 indicates the increase in volume fraction of Laves phase with decreasing temperature. Since at 650 °C a volume fraction of the Laves phase is lower than at 625 °C, a depletion of Mo and W in solid solution at the higher temperature can be expected to be lower. The effects of the differences in volume fraction of other precipitates ($M_{23}C_6$ and MX) at the respective temperatures on the creep behaviour are likely to be negligible.

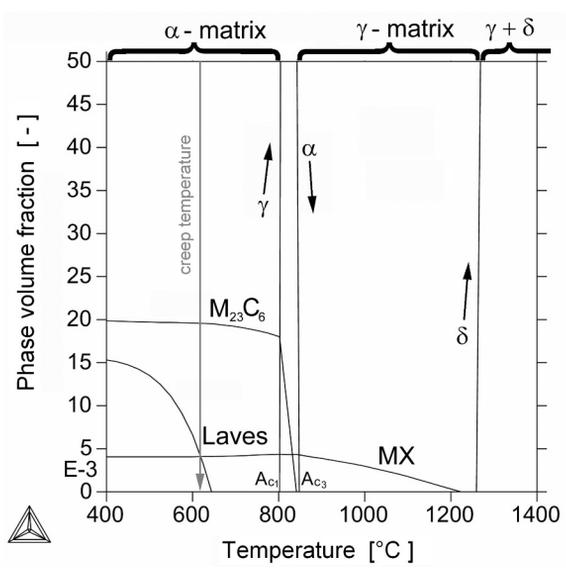

Figure 13. *Calculated stable phases in T91 steel.*

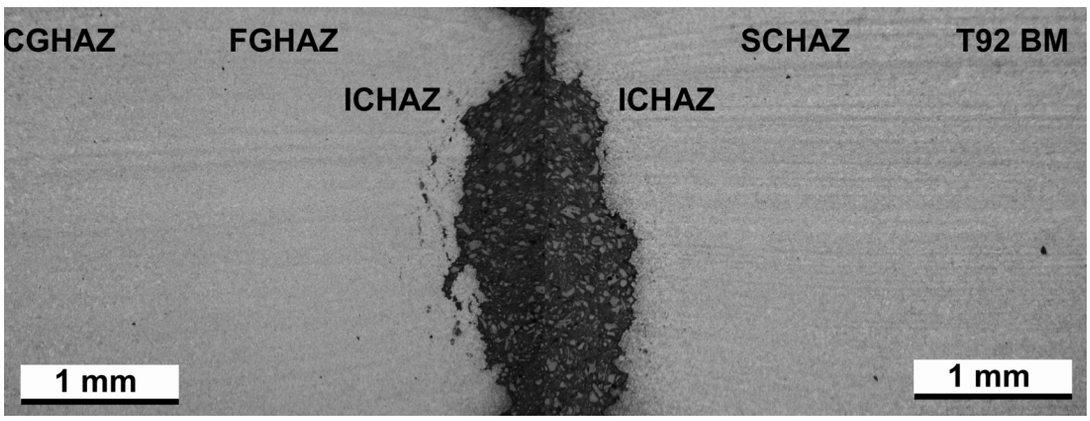

Figure 14. *Light optical microstructures of two counter-parts of the T92+AISI316H weld-joint ruptured by „type IV cracking" after 4060 h at 625 °C / 100 MPa.*

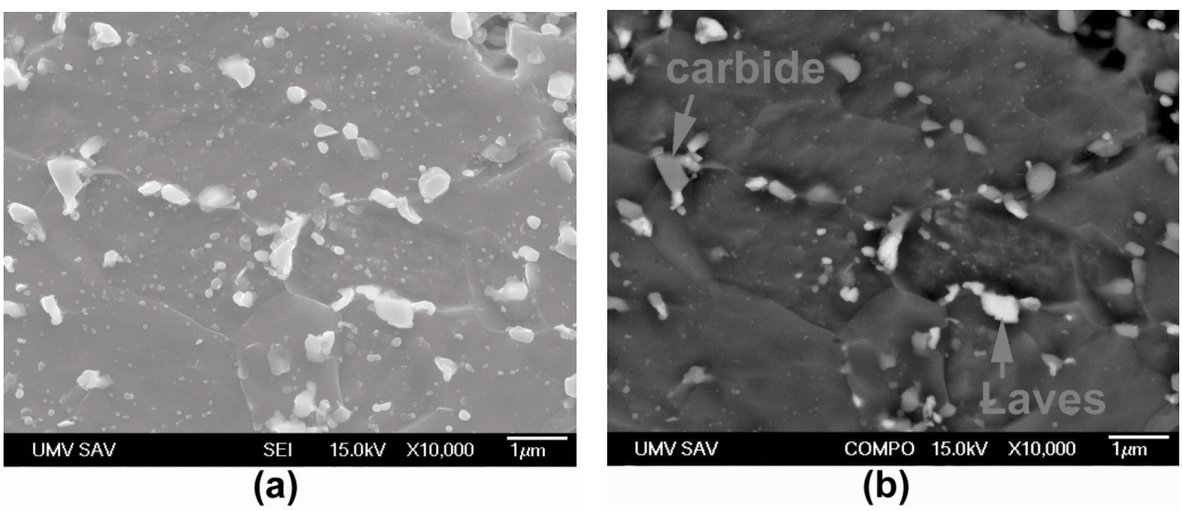

Figure 15. *SEM microstructure of T92 ICHAZ visualised by the contrast of secondary electrons (a) and back-scattered electrons (b).*

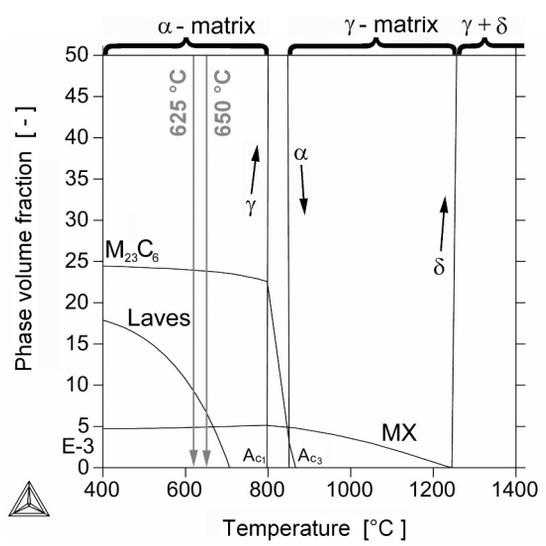

Figure 16. *Calculated stable phases in T92 steel.*

The creep resistance of the studied weld joints was characterised by the dependencies of creep life (time-to-fracture) on applied stress (see Fig. 17). It is evident that at both testing temperatures the creep resistance of the weldment *T92+AISI316H* is significantly better than that of the weldment *T91+AISI316H*. This result can be attributed to the alloying of *T92* steel by tungsten which thermally stabilises the $Fe_2(W,Mo)$ Laves phase (see Fig. 16), compared to the Fe_2Mo Laves phase (see Fig. 13) in *T91* steel without tungsten. However, in comparison with the *T91* and *T92* base materials [21], the creep strength of the corresponding dissimilar weldments is always lower (see Fig. 17) which is directly related to the ICHAZ microstructure degradation (Figs. 12a and 15) leading to the final type IV creep failure.

4. Conclusions

In this work dissimilar ferritic/austenitic

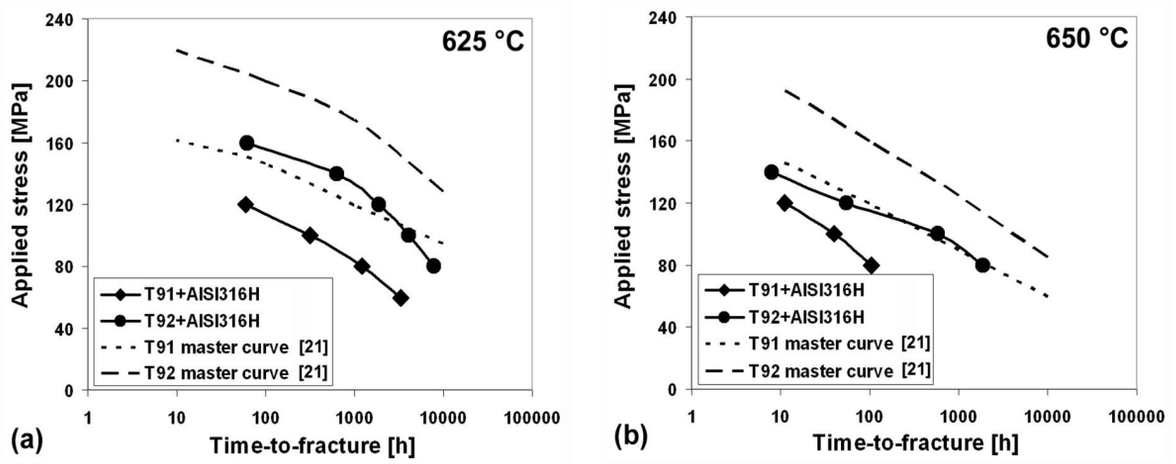

Figure 17. *Creep-rupture data of the studied weldments tested at 625 °C (a) and 650 °C (b) in comparison to the corresponding base materials.*

weldments between 9Cr tempered martensitic steels and unstabilised *AISI316H* austenitic steel were investigated.

Microstructure observations revealed significant heterogeneity within the wide-spread heat-affected zone () of 9Cr steels, whereas the region of *AISI316H* steel was found to be relatively uniform and limited to only a narrow area.

Microstructural gradient in regions of 9Cr steels remained preserved during creep expositions which resulted in premature type IV failure within the intercritical regions of the welded joints.

The most significant microstructural change during creep was the precipitation of intermetallic Laves phase. Experimentally determined phase compositions of the samples after creep exposure are in good agreement with equilibrium thermodynamic calculations.

Acknowledgements

The experimental welded joints were fabricated by the company SES a. s. Tlmače, Slovakia. The performed research work was financially supported by the national projects VEGA 2/0128/10 and VEGA 2/0153/12 of the Slovak Scientific Grant agency.

References

[1] H. Cerjak, P. Mayr, in Creep-resistant steels (F. Abe, T.-U. Kern, R. Viswanathan), Woodhead publishing Ltd, Cambridge, 2008, p.472-503.

[2] V. Knežević, J. Balun, G. Sauthoff, G. Inden, A. Schneider, Mater. Sci. Eng. A, 477 (1–2) A (2008) 334-343.

[3] J. Micheľ, M. Mihaliková, Acta Metall. Slovaca 6 (2) (2000) 108-115.

[4] M. Igarashi, in Creep-resistant steels (F. Abe, T.-U. Kern, R. Viswanathan), Woodhead publishing Ltd, Cambridge, 2008, p.541.

[5] P. Zifčák, P. Brziak, M. Balog, J. Bošanský, M. Srnka, Acta Metall. Slovaca, 14 (2) (2008) 195-208.

[6] S. Caminada, G. Cumino, L. Cipolla, D. Venditti, A. Di Gianfrancesco, Y. Minami, T. Ono, Int. J. Press Ves Piping, 87 (6) (2010) 336-344.

[7] E. Ranjbarnodeh, S. Weis, S. Hanke, A. Fischer, J. Min. Metall. Sect. B-Metall., 48 (1) B (2012) 115-121.

[8] A. K. Bhaduri, S. Venkadesan, P. Rodriguez, P. G. Mukunda, Int. J. Press. Ves. Piping 58 (3) (1994) 251–265.

[9] Ľ. Dobrovský, L. Řeháčková, J. Dobrovská, K. Stránský, V. Dobrovská, Acta Metall. Slovaca 11 (3) (2005) 259-265.

[10] V. Pilous, K. Stránský, Structural stability of deposits and welded joints in power engineering, Cambridge International Science Publication, Cambridge, 1998, p.13.

[11] www.thermocalc.se

[12] A. Kroupa, Internal report of IPM Brno 2006

[13] A. Kroupa, J. Havránková, M. Coufalová, M. Svoboda, J. Vrešťál, J. of Phase Equil. 22 (2001) 312-323.

[14] J. Blach, Kovove Mater., 38 (5) (2000) 315–328.

[15] L. Falat, A. Výrostková, M. Svoboda, O. Milkovič, Kovove Mater., 49 (6) (2011) 417-426.

[16] G. Eggeler, A. Ramteke, M. Coleman, B. Chew, G. Peter, A. Burblies, J. Hald, C. Jefferey, J. Rantala, M. deWitte, R. Mohrmann, Int. J. Press. Ves. Piping, 60 (3) (1994) 237-257.

[17] L. Kloc, V. Sklenička, Mater. Sci. Eng. A, 234-236 A (1997) 962–965.

[18] P. J. Ennis, A. Zielinska-Lipiec, O.Wachter, A. Czyrska-Filemonowicz, Acta Mater., 45 (12) (1997) 4901-4907.

[19] J. S. Lee, H. G. Armaki, K. Maruyama, T. Muraki, H. Asahi, Mater. Sci. Eng., A 428 (1-2) A (2006) 270-275.

[20] K. Sawada, K. Kubo, F. Abe, Mater. Sci. Eng., A 319-321 A (2001) 784-787.

[21] T. Massé, Y. Lejeail, Nucl. Eng. Des., 246 (2012) 220-232.